A fixed-point current injection power flow for electric distribution systems using Laurent series

Article *in* Electric Power Systems Research · October 2022

DOI: 10.1016/j.epsr.2022.108326

CITATION
1

READS
46

4 authors:

Juan S. Giraldo
TNO
37 PUBLICATIONS **217** CITATIONS
SEE PROFILE

Oscar Danilo Montoya Giraldo
Universidad Tecnológica de Bolívar
259 PUBLICATIONS **2,103** CITATIONS
SEE PROFILE

Pedro P. Vergara
Delft University of Technology
54 PUBLICATIONS **457** CITATIONS
SEE PROFILE

Federico Milano
University College Dublin
355 PUBLICATIONS **7,758** CITATIONS
SEE PROFILE

Electric Power Systems Research 211 (2022) 108326

Contents lists available at ScienceDirect

Electric Power Systems Research

journal homepage: www.elsevier.com/locate/epsr

A fixed-point current injection power flow for electric distribution systems using Laurent series

Juan S. Giraldo [a,*], Oscar Danilo Montoya [c,d], Pedro P. Vergara [b], Federico Milano [e]

[a] dept. Electrical Engineering, Mathematics, and Computer Science – University of Twente, The Netherlands
[b] Intelligent Electrical Power Grids Group – Delft University of Technology, The Netherlands
[c] Universidad Distrital Francisco José de Caldas, Colombia
[d] Universidad Tecnológica de Bolivar, Colombia
[e] School of Electrical & Electronic Engineering – University College Dublin, Ireland

ARTICLE INFO

Keywords:
Current injection power flow
Laurent series
Fixed-point iteration
Three-phase systems

ABSTRACT

This paper proposes a new power flow (PF) formulation for electrical distribution systems using the current injection method and applying the Laurent series expansion. Two solution algorithms are proposed: a Newton-like iterative procedure and a fixed-point iteration based on the successive approximation method (SAM). The convergence analysis of the SAM is proven via the Banach fixed-point theorem, ensuring numerical stability, the uniqueness of the solution, and independence on the initializing point. Numerical results are obtained for both proposed algorithms and compared to well-known PF formulations considering their rate of convergence, computational time, and numerical stability. Tests are performed for different branch R/X ratios, loading conditions, and initialization points in balanced and unbalanced networks with radial and weakly-meshed topologies. Results show that the SAM is computationally more efficient than the compared PFs, being more than ten times faster than the backward–forward sweep algorithm.

1. Introduction

1.1. Motivation

It is well-known that specific system characteristics might create numerical issues for certain PF formulations, decreasing their convergence speed or even causing them to diverge [1]. For instance, high R/X branch ratios, the loading condition, and poor initialization have been identified as potential reasons for numerical instabilities in several formulations, commonly known as ill-conditioned cases [2]. Electric distribution systems are characterized by high R/X branch ratios and unbalanced operation in medium/low voltage levels, making them good candidates to present numerical instabilities. Hence, although it is a well-studied subject, finding scalable, computationally efficient, and numerically stable PF algorithms for distribution networks is still of interest to the power systems community.

1.2. Literature review

Classical PF algorithms in transmission systems rely mainly on the Newton–Raphson (NR) method or its decoupled versions [3]. However, some particularities of distribution systems, such as their radiality, unbalanced operation, mixed loading models, and the number of nodes and branches, motivate the formulation of specific solution methods exploding such characteristics, e.g., the backward–forward sweep method (BFS) [4]. The convergence of the BFS for different load models has been studied in [1], where it was found that it is related to the magnitude of the equivalent line impedance and load admittance, but it is not highly affected by the load power factor. Similarly, the current injection method (CIM) was proposed in [5] for unbalanced three-phase networks using a Newton-like scheme. Results showed that the CIM converges in fewer iterations than the BFS, especially under heavy-load conditions and is practical for ill-conditioned cases [6]. Furthermore, the Jacobian matrix presents some interesting properties over the classical NR formulation, such as a reduced number of elements that need to be updated. Substantial work has been done towards solving ill-conditioned cases, such as in [2,7] using the implicit continuous Newton method (ICN), in [8] using an NR with step-size optimization (Braz), in [9] using a second-order approximation and the Levenberg–Marquardt (LM) method, or using Runge–Kutta formulas as in [10].

The Laurent series expansion is a representation of a complex function as a power series and can be seen as an extension of Taylor

* Corresponding author.
E-mail address: jnse@ieee.org (J.S. Giraldo).

https://doi.org/10.1016/j.epsr.2022.108326
Received 17 September 2021; Received in revised form 17 February 2022; Accepted 2 July 2022
Available online 13 July 2022

series at singularity points [11]. The use of Laurent series expansions for solving the PF problem was first introduced in [12] to obtain a linear non-iterative solution using the CIM. Still, it approximates over a single operating point ($1\angle 0$), meaning its accuracy might be affected by the loading condition and branches R/X ratio. More recently, authors in [13] proposed an iterative formulation using Laurent series expansion to linearize the product of variables, showing computational improvements over the classical NR method and equivalent results to the BFS. Nevertheless, it was only tested in one-line equivalent networks, disregarding different load models.

A recent class of PF formulations based on fixed-point iterations have been proposed in the literature. A linear approximation is introduced in [14] where the authors have derived a sufficient condition for the existence of a practical solution to the PF in balanced distribution systems using the Banach fixed point theorem. Authors in [15] extended these findings to unbalanced three-phase networks using the Z-bus iterative method providing four conditions that guarantee the convergence to a unique solution. Multiphase systems are dealt with in [16], where a condition for the non-singularity of the load-flow Jacobian is presented. In [17], the authors proposed a successive approximation method based on a modification of the Gauss–Seidel PF for radial and meshed networks showing computational improvements over the compared algorithms. A fixed-point iteration is described in [18] to solve the PF problem iteratively without matrix inversions. However, the formulation is suitable only for single-line equivalent networks, and the rate of convergence is low, requiring almost 100 iterations to achieve mismatches of 0.001 pu. Finally, authors in [19] proposed a derivative-free fixed-point method based on the upper-triangular-based PF with better convergence properties; however, it only works for radial networks.

1.3. Contributions

This paper proposes a novel PF formulation for electrical distribution systems using the CIM and applying the Laurent series expansion. Since it is based on the admittance matrix and nodal current injections, the proposed formulation can cope with radial and weakly-meshed topologies. This paper proposes two solution algorithms: a Newton-like iterative procedure named direct solution (DS) and a successive approximation method (SAM). The convergence analysis of the SAM is proven via the Banach fixed-point theorem, ensuring numerical stability and the uniqueness of the solution regardless of the initializing point. Compared to [15] or [16], this paper extends the solution to weakly-meshed networks and introduces an inductive physical interpretation to the mathematical proof by relating the existence and uniqueness of the PF solution to the physical operating point in terms of static voltage stability. Results are obtained for both proposed algorithms and compared to well-known PF algorithms in terms of rate of convergence, computational time, and numerical stability. Several tests are performed considering different branch R/X ratios, loading conditions, and initialization points. Finally, the scalability of the formulations is assessed using balanced and unbalanced networks ranging from 33 to 3120 buses.

2. Current injection power flow method

Consider a system with a set of nodes represented as Ω_B. $\boldsymbol{Y}$ is the three-phase admittance submatrix of size $\Omega_B \times \Omega_B$, composed by constant voltage nodes (s) and load nodes (d), such as $s, d \subset \Omega_B$ as:

where $\boldsymbol{Y}_{sd}^T = \boldsymbol{Y}_{ds}$. The relationship between voltages and currents is expressed using Kirchhoff's laws as:

$$\begin{bmatrix} \boldsymbol{I}_s \\ -\boldsymbol{I}_d \end{bmatrix} = \begin{bmatrix} \boldsymbol{Y}_{ss} & \boldsymbol{Y}_{sd} \\ \boldsymbol{Y}_{ds} & \boldsymbol{Y}_{dd} \end{bmatrix} \begin{bmatrix} \boldsymbol{V}_s \\ \boldsymbol{V}_d \end{bmatrix} \tag{1}$$

where vectors $\boldsymbol{I}_s$ and $\boldsymbol{I}_d$ represent three-phase complex nodal current injections, while $\boldsymbol{V}_s$ and $\boldsymbol{V}_d$ the three-phase complex components of the nodal voltages.

It must be noticed that $\boldsymbol{V}_s = \left[1, a^2, a\right]$, for all constant voltage nodes, unless specifically stated, with $a = e^{j2\pi/3}$ hereinafter. Additionally, the current injection at load nodes ($\boldsymbol{I}_d$) is a function of the complex power injection $\boldsymbol{S}_d$, accounting for loads and renewable energy resources at each bus directly since they are considered as constant power injections. Hence, the system of equations has an equal number of equations and unknowns but is nonlinear due to (2b):

$$\mathbf{diag}\left(\boldsymbol{V}_s^*\right)^{-1} \boldsymbol{S}_s^* = \boldsymbol{Y}_{ss}\boldsymbol{V}_s + \boldsymbol{Y}_{sd}\boldsymbol{V}_d \tag{2a}$$

$$-\mathbf{diag}\left(\boldsymbol{V}_d^*\right)^{-1} \boldsymbol{S}_d^* = \boldsymbol{Y}_{ds}\boldsymbol{V}_s + \boldsymbol{Y}_{dd}\boldsymbol{V}_d \tag{2b}$$

where $\mathbf{diag}(\cdot)$ represents a squared diagonal matrix. Let $\boldsymbol{I}_d = \left[i_{i,\phi}^{re} + \mathrm{j}\, i_{i,\phi}^{im}\right]$ be the vector containing the current injection at each load node $i \in d$ and phase $\phi \in \Omega_\Phi$. Similarly, take $\boldsymbol{V}_d = \left[v_{i,\phi}^{re} + \mathrm{j}\, v_{i,\phi}^{im}\right]$, and $\boldsymbol{S}_n = \left[\mathrm{P}_{i,\phi} + \mathrm{jQ}_{i,\phi}\right]$, representing the voltage and nominal complex power, respectively. In order to consider the ZIP load model, nodal loads are defined as:

$$\boldsymbol{S}_d = \left(\mathbf{diag}\left(\alpha_P\right) + \mathbf{diag}\left(\alpha_I \boldsymbol{V}_d\right) + \mathbf{diag}\left(\alpha_Z |\boldsymbol{V}_d|^2\right)\right) \boldsymbol{S}_n \tag{3}$$

Hence, considering that $\boldsymbol{S}_d = \boldsymbol{V}_d \boldsymbol{I}_d^*$, nodal currents' components are expressed as:

$$\boldsymbol{I}_d = \left(\alpha_P \mathbf{diag}\left(\boldsymbol{V}_d^*\right)^{-1} + \mathbf{diag}\left(\alpha_I\right) + \alpha_Z \mathbf{diag}\left(\boldsymbol{V}_d\right)\right) \boldsymbol{S}_n^* \tag{4}$$

where α_Z, α_I, and α_P represent the ZIP coefficients per load node and phase. Notice that the ZIP model implemented has a constant-current-phasor representation as in [12]; thus, it is linear for constant current and constant impedance loads in the presented formulation. Hence, the proposed formulation is not an approximation to the traditional PF, and the nonlinearity is introduced by the constant power load component.

3. Linear approximation with Laurent series

A linear expression for (4) could be obtained using first-order Taylor series expansion as in [5] since it satisfies the Cauchy–Riemann equations. However, the proposed approach uses Laurent series to approximate the complex domain since it provides a more general and condensed representation. A Laurent series is a complex-differentiable function on the annulus $r_1 < |z - z_0| < r_2$ of the form:

$$f(z) = \sum_{n=0}^{\infty} a_n \left(z - z_0\right)^n + \sum_{n=1}^{\infty} \frac{b_n}{\left(z - z_0\right)^n} \tag{5}$$

where z is a complex number, while a_n and b_n are defined by a line integral generalizing the Cauchy's integral formula, and z_0 is a complex number located at the center of the annulus [11]. In particular, it is said that the first component of $f(z)$ converges to an analytic solution for $|z - z_0| < r_2$, while the second one converges to an analytic solution for $|z - z_0| > r_1$. Based on these conditions, we propose the following:

Proposition 1. *The nonlinearity introduced by the expression $f(V_i) = \left(V_i\right)^{-1}$ at a node $i \in d$, is approximated around $\mathrm{V}^0 \in \mathbb{C}$ using Laurent series expansion assuming $V_i = \mathrm{V}^0 - \Delta V$, as $f(V_i) \approx 2/\mathrm{V}^0 - V_i/\mathrm{V}^{0^2}$.*

Proof. Function $f(\Delta V)$ can be expressed with the following power series, with $\xi = \|\Delta V\| \,/\, \left\|\mathrm{V}^0\right\|$

$$f(\Delta V) = \frac{1}{\mathrm{V}^0 - \Delta V} = \begin{cases} \sum_{n=0}^{\infty} \frac{-\mathrm{V}^{0^n}}{\Delta V^{n+1}} & \text{for } \xi > 1.0 \\ \sum_{n=1}^{\infty} \frac{\Delta V^{n-1}}{\mathrm{V}^{0^n}} & \text{for } \xi < 1.0 \end{cases} \tag{6}$$

Assumption 1. Voltages are expected to exist within a close boundary, as depicted in Fig. 1. Thus, after assuming $\xi < 1.0$, $f(\Delta V)$ can be rewritten as

$$f(\Delta V) = \frac{1}{\mathrm{V}^0} + \frac{\Delta V}{\mathrm{V}^{0^2}} + \mathcal{O} \tag{7}$$

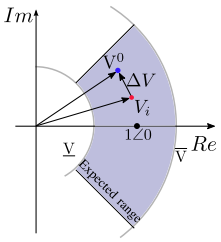

Fig. 1. Graphical representation of Assumption 1.

where $\mathcal{O}$ represents the high order terms. Hence, the first order approximation ($n \leq 2$) in terms of the nodal voltage reads

$$f(V_i) \approx \frac{2}{\mathrm{V}^0} - \frac{V_i}{\mathrm{V}^{0^2}}. \quad \square \tag{8}$$

By applying Proposition 1, nodal currents at a node $i \in d$ are approximated as:

$$\boldsymbol{I}_{i,\phi} = \left[\alpha_{P,i,\phi}\left(2\,\mathbf{V}_{i,\phi}^{0\ -1} - \mathbf{V}_{i,\phi}^{0\ -2}\boldsymbol{V}_{i,\phi}\right)^* + \alpha_{I,i,\phi} + \alpha_{Z,i,\phi}\boldsymbol{V}_{i,\phi}\right]\boldsymbol{S}_{n,i}^*. \tag{9}$$

It should be pointed out that (9) is a general approximation for any operational point $\mathbf{V}^0 = \left[\mathbf{V}_{i,\phi}^0\right]$. Proposition 1 can be extended to a three-phase representation; thus, it can be seen that a particular case with $\mathbf{V}_{i,\phi}^0 = \left[1,\, a^2,\, a\right] \forall i \in d$ is equivalent to the linear non-iterative approximation proposed in [12].

4. Proposed algorithms

The following system of linear equations is obtained after substituting (9) in (2):

$$\boldsymbol{A}\boldsymbol{V}_d^* - \boldsymbol{B}\boldsymbol{V}_d = \boldsymbol{C} + \boldsymbol{D} \tag{10}$$

where

$$\boldsymbol{A} = \mathbf{diag}\left(\alpha_P \odot \mathbf{V}^{0^{*-2}} \odot \boldsymbol{S}_n^*\right) \tag{11a}$$

$$\boldsymbol{B} = \mathbf{diag}\left(\alpha_Z \odot \boldsymbol{S}_n^*\right) + \boldsymbol{Y}_{dd} \tag{11b}$$

$$\boldsymbol{C} = \boldsymbol{Y}_{ds}\boldsymbol{V}_s + \alpha_I \odot \boldsymbol{S}_n^* \tag{11c}$$

$$\boldsymbol{D} = 2\,\alpha_P \odot \mathbf{V}^{0^{*-1}} \odot \boldsymbol{S}_n^* \tag{11d}$$

with $\odot$ representing the Hadamard product, and $\mathbf{V}^{0^{*-1}}$ representing the element-wise inverse of vector $\mathbf{V}^0$ conjugate. This paper proposes two alternatives for solving the system of linear equations in (10):

4.1. Direct Solution (DS)

The complex expression in (10) can be rewritten as:

$$\begin{bmatrix} \boldsymbol{M}_{11} & \boldsymbol{M}_{12} \\ \boldsymbol{M}_{21} & \boldsymbol{M}_{22} \end{bmatrix}\begin{pmatrix} \boldsymbol{V}_d^{re} \\ \boldsymbol{V}_d^{im} \end{pmatrix} = \begin{pmatrix} \boldsymbol{C}^{re} + \boldsymbol{D}^{re} \\ \boldsymbol{C}^{im} + \boldsymbol{D}^{im} \end{pmatrix} \tag{12}$$

where superscripts *re* and *im* stand for the real and imaginary components of each matrix. Notice that matrices $\boldsymbol{M}_{11} = \boldsymbol{A}^{re} - \boldsymbol{B}^{re}$, $\boldsymbol{M}_{12} = \boldsymbol{A}^{im} + \boldsymbol{B}^{im}$, $\boldsymbol{M}_{21} = \boldsymbol{A}^{im} - \boldsymbol{B}^{im}$, and $\boldsymbol{M}_{22} = -\boldsymbol{A}^{re} - \boldsymbol{B}^{re}$.

An iterative method to solve the linear three-phase PF problem in (10) is given in Algorithm 1 assuming flat-start. A similar procedure can be performed for balanced single-line equivalents. It must be pointed out that $\boldsymbol{B}$ and $\boldsymbol{C}$ do not change within the iterative process; hence, only $\boldsymbol{A}^{(k)}$ and $\boldsymbol{D}^{(k)}$ need to be updated. Thus, the algorithm converges in only one iteration if $\alpha_P = \mathbf{0}$. Moreover, similar to the Jacobian in [5], only the diagonals of the submatrices in $\boldsymbol{M}$ need to be updated at each iteration. In fact, note that the proposed algorithm is a compacted, simpler form of the one introduced in [5].

Algorithm 1 Direct Solution (DS)

1: Initialize $k = 0$, $tol > \epsilon$
2: Initialize $\mathbf{V}_{i,\phi}^0 = \left[1,\, a^2,\, a\right]\ \forall i \in d$
3: Compute $\boldsymbol{B}$ and $\boldsymbol{C}$
4: **while** $tol \geq \epsilon$ **and** $k \leq K$:
5: Compute $\boldsymbol{A}^{(k)}$, and $\boldsymbol{D}^{(k)}$
6: Solve for $\boldsymbol{V}_d^{(k+1)}$:

$$\begin{bmatrix} \boldsymbol{M}_{11}^{(k)} & \boldsymbol{M}_{12}^{(k)} \\ \boldsymbol{M}_{21}^{(k)} & \boldsymbol{M}_{22}^{(k)} \end{bmatrix}\begin{pmatrix} \boldsymbol{V}_d^{re(k+1)} \\ \boldsymbol{V}_d^{im(k+1)} \end{pmatrix} = \begin{pmatrix} \boldsymbol{C}^{re} + \boldsymbol{D}^{re^{(k)}} \\ \boldsymbol{C}^{im} + \boldsymbol{D}^{im^{(k)}} \end{pmatrix}$$

7: $-\boldsymbol{S}_d^{*(k+1)} = \mathbf{diag}\left(\boldsymbol{V}_d^{*(k+1)}\right)\left(\boldsymbol{Y}_{ds}\boldsymbol{V}_s + \boldsymbol{Y}_{dd}\boldsymbol{V}_d^{(k+1)}\right)$
8: $tol \leftarrow \max\left\|\boldsymbol{S}_d^* - \boldsymbol{S}_d^{*(k+1)}\right\|$
9: $\mathbf{V}^0 \leftarrow \boldsymbol{V}_d^{(k+1)}$
10: $k \leftarrow k+1$
11: Compute $\boldsymbol{S}_s^* = \mathbf{diag}\left(\boldsymbol{V}_s^*\right)\left(\boldsymbol{Y}_{ss}\boldsymbol{V}_s + \boldsymbol{Y}_{sd}\boldsymbol{V}_d^{(k)}\right)$
12: **Return:** $\boldsymbol{V}_d^{(k)}$, $\boldsymbol{S}_s$

4.2. Successive Approximation Method (SAM)

The system of linear equations in (10) can be rearranged as:

$$\boldsymbol{V}_d = \boldsymbol{B}^{-1}\left(\boldsymbol{A}\boldsymbol{V}_d^* - \boldsymbol{C} - \boldsymbol{D}\right). \tag{13}$$

The set of equations in (13) presents a typical structure to apply the Banach fixed-point theorem for solving roots in nonlinear problems. Notice that (13) is a function of the form

$$\boldsymbol{V}_d^{(k+1)} = f\left(\boldsymbol{V}_d^{(k)}\right), \tag{14}$$

leading to

$$\boldsymbol{V}_d^{(k+1)} = \boldsymbol{B}^{-1}\left(\boldsymbol{A}^{(k)}\boldsymbol{V}_d^{*(k)} - \boldsymbol{C} - \boldsymbol{D}^{(k)}\right). \tag{15}$$

An iterative method to solve the PF using the SAM is shown in Algorithm 2. It should be highlighted that the successive solution of (15) requires a single matrix inversion, whose values do not change in the iterative process. Obtaining $\boldsymbol{B}^{-1}$ by direct inversion can be a challenge in large networks; however, efficient building algorithms can be used [20]. Moreover, $\boldsymbol{B}^{-1}$ can be factorized (e.g., LDU), stored, and only updated in case of topological changes or demand variations in constant impedance loads. This particularity presents a potential computational advantage over other methods that rely on matrix inversions within the iterative process to obtain the result of the PF, e.g., NR, Braz, or DS. It is also noteworthy that the main difference with the BFS is that the SAM uses the current injection method instead of branch current flows. This difference allows directly considering weakly-meshed networks and not relying on a specific node sequence enumeration. The code implementations of the DS and SAM algorithms for balanced and unbalanced networks can be found in [21].

Furthermore, it can be demonstrated that (15) is a contraction mapping. Hence, the convergence of Algorithm 2 can be analyzed using the Banach fixed-point theorem as in [17]. Let $\mathbb{U}_d$ represent the exact solution of the PF, i.e., a vector containing the voltages of the demand nodes at all phases, and $\underline{v}$ the minimum voltage magnitude, i.e., $\underline{v} = \min_{i\in d}\left\|u_i\right\|$ with $u_i \in \mathbb{U}_d$.

Proposition 2. *Algorithm 2 is a contraction mapping of the form* $\boldsymbol{V}_d^{(k+1)} = f\left(\boldsymbol{V}_d^{(k)}\right)$*; hence, it is stable and has unique solution for any initial value* $\boldsymbol{V}_d^0$ *if*

$$\left\|f\left(\boldsymbol{V}_d^{(k)}\right) - f\left(\mathbb{U}_d\right)\right\| \leq \eta\left\|\boldsymbol{V}_d^{(k+1)} - \mathbb{U}_d\right\| \tag{16}$$

Algorithm 2 Successive Approximation Method (SAM)

1: Initialize $k = 0$, $tol > \epsilon$
2: Initialize $\mathbf{V}_{i,\phi}^{0} = [1, a^2, a]\ \forall i \in d$
3: Compute $\boldsymbol{B}^{-1}$ and $\boldsymbol{C}$
4: **while** $tol \geq \epsilon$ **and** $k \leq K$:
5: Compute $\boldsymbol{A}^{(k)}$, and $\boldsymbol{D}^{(k)}$
6: Solve for $\boldsymbol{V}_d^{(k+1)}$:

$$\boldsymbol{V}_d^{(k+1)} = \boldsymbol{B}^{-1}\left(\boldsymbol{A}^{(k)}\mathbf{V}_d^{*0} - \boldsymbol{C} - \boldsymbol{D}^{(k)}\right)$$

7: $-\boldsymbol{S}_d^{*(k+1)} = \mathbf{diag}\left(\boldsymbol{V}_d^{*(k+1)}\right)\left(\boldsymbol{Y}_{ds}\boldsymbol{V}_s + \boldsymbol{Y}_{dd}\boldsymbol{V}_d^{(k+1)}\right)$
8: $tol \leftarrow \max\left\|\boldsymbol{S}_d^{*} - \boldsymbol{S}_d^{*(k+1)}\right\|$
9: $\mathbf{V}_d^{0} \leftarrow \boldsymbol{V}_d^{(k+1)}$
10: $k \leftarrow k+1$
11: Compute $\boldsymbol{S}_s^{*} = \mathbf{diag}\left(\boldsymbol{V}_s^{*}\right)\left(\boldsymbol{Y}_{ss}\boldsymbol{V}_s + \boldsymbol{Y}_{sd}\boldsymbol{V}_d^{(k)}\right)$
12: **Return:** $\boldsymbol{V}_d^{(k)}$, $\boldsymbol{S}_s$

where

$$\eta = \max\left\{\frac{\left\|\boldsymbol{B}^{-1}\,\mathbf{diag}\left(\alpha_P \odot \boldsymbol{S}_n^{*}\right)\right\|}{\underline{v}^2}\right\}, \quad 0 \leq \eta < 1. \tag{17}$$

Proof. Based on the Banach fixed-point theorem, the fixed-point $\mathbb{U}_d$ satisfying $f\left(\mathbb{U}_d\right) = \mathbb{U}_d$ exists and is unique if $f\left(\mathbb{U}_d\right)$ is a contraction mapping on $\mathbb{U}_d$; thus:

$$\begin{aligned}\left\|\boldsymbol{V}_d^{(k+1)} - \mathbb{U}_d\right\| &= \left\|f\left(\boldsymbol{V}_d^{(k)}\right) - f\left(\mathbb{U}_d\right)\right\| \\ &= \left\|\boldsymbol{B}^{-1}\boldsymbol{A}^{(k)}\left(\boldsymbol{V}_d^{*(k)} - \mathbb{U}_d^{*}\right)\right\|\end{aligned} \tag{18}$$

since $\boldsymbol{A}^{(k)}$ is a diagonal matrix, we have

$$\begin{aligned}\left\|\boldsymbol{V}_d^{(k+1)} - \mathbb{U}_d\right\| &\leq \frac{\left\|\boldsymbol{B}^{-1}\,\mathbf{diag}\left(\alpha_P \odot \boldsymbol{S}_n^{*}\right)\right\|}{\left\|\boldsymbol{V}_d^{*(k)}\right\|^2}\left\|\boldsymbol{V}_i^{*(k)} - \mathbb{U}_i^{*}\right\|_{i\in d} \\ &\leq \eta\left\|\boldsymbol{V}_d^{*(k)} - \mathbb{U}_d^{*}\right\|\end{aligned} \tag{19}$$

hence, if the solution exists, then

$$\eta = \max\left\{\frac{\left\|\boldsymbol{B}^{-1}\,\mathbf{diag}\left(\alpha_P \odot \boldsymbol{S}_n^{*}\right)\right\|}{\left\|\mathbb{U}_d\right\|^2}\right\} \text{ with } 0 \leq \eta < 1. \tag{20}$$

Thus, two conditions need to be satisfied $\underline{v} > 0$ and $\left\|\boldsymbol{B}^{-1}\,\mathbf{diag}\left(\alpha_P \odot \boldsymbol{S}_n^{*}\right)\right\| < \underline{v}^2$.

Assumption 2. Matrix $\boldsymbol{B}$ is full rank, and is hence invertible [22]; thus, $\boldsymbol{Z} = \boldsymbol{B}^{-1}$, where $\boldsymbol{Z}_{ij}$ is the impedance between nodes ij.

Assuming $\alpha_{P_i} = 1$ and defining $\boldsymbol{ZL}_i = \underline{v}^2 / \left\|\boldsymbol{S}_n^{*}\right\|_i$ as the load impedance at each node using the lowest voltage of the system. Considering that $\boldsymbol{Z}_{ii} \geq \boldsymbol{Z}_{ij}$, then $\eta \approx \max_{i\in d}\left\{\left\|\boldsymbol{Z}_{ii}/\boldsymbol{ZL}_i\right\|\right\}$. The second condition can be rewritten as

$$\left\|\boldsymbol{Z}_{ii}\right\| < \left\|\boldsymbol{ZL}_i\right\|, \forall i \in d. \tag{21}$$

The first condition ($\underline{v} > 0$) can be ensured since voltage magnitudes are greater than zero in normal operation, implying that the PF equations can be solved. The second condition can also be satisfied since $\boldsymbol{Z}_{ii}$ is the Thevenin impedance as seen from node i, while $\boldsymbol{ZL}_i$ denotes the maximum loading impedance at node i for a given operating point. According to the maximum power transfer theorem, the maximum loading impedance at a node is lower than its Thevenin impedance (except at the maximum loading point where they are numerically identical [23]). Since both conditions can be satisfied in normal operation, then $f\left(\boldsymbol{V}_d\right)$ is a contraction mapping on $\boldsymbol{V}_d$ which completes the proof. □

Notice that Proposition 2 is coherent with the conditions on the existence and uniqueness of PF solutions in distribution systems described in [15,24]. It should also be remarked that smaller values of η mean higher rates of convergence. In this sense, $\eta = 0$ implies that $\alpha_P = \mathbf{0}$, indicating that the solution is analytical if loads are modeled as a combination of constant current and constant impedances. Instead, notice that (10) can also be rearranged as $\boldsymbol{V}_d^{(k+1)*} = \boldsymbol{A}^{(k)^{-1}}\left(\boldsymbol{BV}_d^{(k)} + \boldsymbol{C} + \boldsymbol{D}^{(k)}\right)$, which would not require inverting the admittance matrix. However, using (16), it can be shown that it is not useful since it is not a contraction mapping on $\boldsymbol{V}_d$, i.e., $\eta > 1$ in normal operation.

5. Tests and results

5.1. Balanced systems

A set of tests are performed in two radial, medium-voltage balanced systems with 34 and 136 buses, whose topology and nominal loading can be found in [25], and [26], respectively. Results are compared with traditional algorithms, namely, NR, BFS, Levenberg–Marquardt method (LM), NR with step size optimization (Braz), Runge–Kutta 4th order method (RK4), and the implicit continuous Newton method (ICN), all of them implemented in the software Dome [27]. The convergence criterion $\epsilon = 10^{-6}$ has been assumed for all algorithms. First, the algorithms' performance to different branch R/X ratios is assessed by comparing the number of iterations to converge. Then, the algorithms' sensitivity to different loading conditions is compared.

5.1.1. Sensitivity to R/X ratio

Tests are performed considering different R/X ratios by scaling each line's resistance with a factor $\rho \in [1.0, 5.0]$. The nominal load condition was assumed, and all algorithms were initialized with a flat-start. The number of iterations required for the tested algorithms to converge is depicted in Fig. 2 for both test systems and two different values of ρ. It can be seen that the proposed DS algorithm converges in fewer iterations than the other tested algorithms, even for high R/X ratios. As a remark, note that the first iteration of the DS algorithm corresponds to the solution of the method proposed in [12].

For instance, in Fig. 2d, the DS and ICN algorithms converged after four iterations, while the NR and Braz converged in 6. Similarly, the LM in 12 iterations, the SAM in 18, the BFS in 19, and the RK4 in 16. However, it should be mentioned that the ICN performs an additional number of iterations due to its inner loop [7]. Moreover, it can be seen that the DS algorithm presents better rates of convergence than the BFS, which is a similar result as in [5]. From Fig. 2 it is also evident that the rate of convergence of the SAM algorithm decreases after increasing the impedance magnitude, i.e., the number of iterations increases. In fact, as can be inferred from (17), increasing the branches' impedance magnitude implies decreasing the rate of convergence, e.g., for the 136-bus test system with $\rho = 1.0$ is $\eta = 0.0757$, while for $\rho = 3.0$ is $\eta = 0.1488$. On the other hand, considering topological meshed systems would increase the rate of convergence since η would be lower.

5.1.2. Sensitivity to loading condition

Tests are performed with $\rho = 1.0$ and scaling all loads in both test systems with a factor $\lambda \in [1.0, \lambda_{\text{mlp}})$, where λ_{mlp} represents the scale factor at the maximum loading point of each system. The maximum loading point of both systems was found with the method described in [8], i.e., when the optimal step size is equal to zero using the Braz step size optimization algorithm. For the 34-bus test system, it was found a $\lambda_{\text{mlp}} = 9.48282$, whereas for the 136-bus test system $\lambda_{\text{mlp}} = 2.45013$. The number of iterations to converge as a function of the loading factor can be seen in Fig. 3 using four different load flow

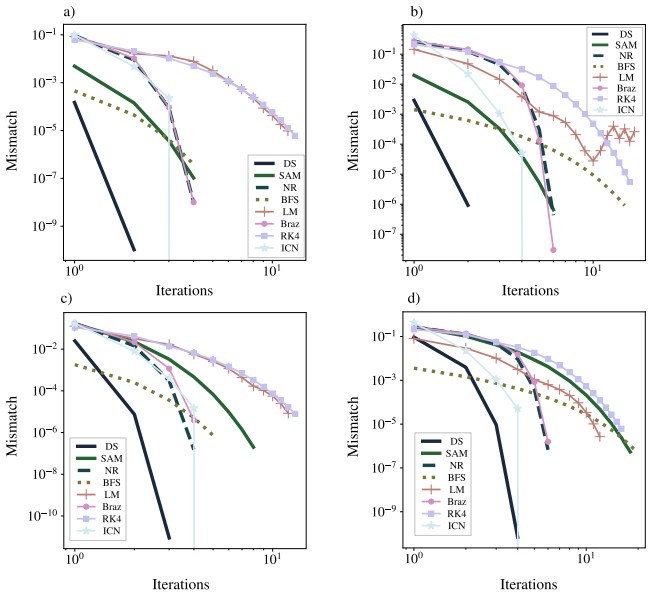

Fig. 2. Power flow performance for different R/X ratios. (a) 34-bus $\rho = 1.0$, (b) 34-bus $\rho = 5.0$, (c) 136-bus $\rho = 1.0$, (d) 136-bus $\rho = 5.0$.

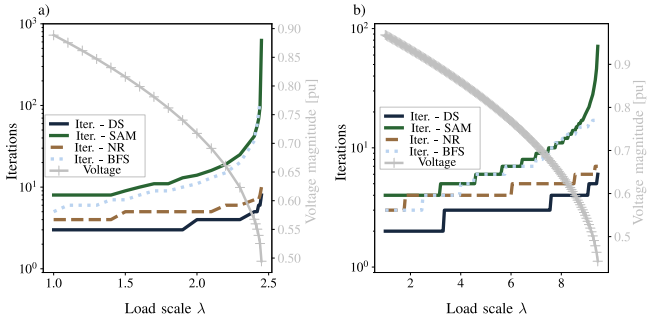

Fig. 3. Power flow performance for different loading conditions. (a) 136-bus, (b) 34-bus.

algorithms. It can be seen that the DS algorithm outperforms all tested algorithms and has a similar performance to the NR since the rate of convergence is not highly affected by the loading condition. On the other hand, the SAM and BFS algorithms present a higher sensitivity to λ, increasing rapidly as the load approaches λ_{mlp}. This behavior can be inferred from (21) for the SAM algorithm since $\eta \approx 1.0$ at the maximum loading point, hence decreasing its rate of convergence.

5.2. Unbalanced systems

Several tests are performed in the IEEE 123-node test feeder, a radial, medium-voltage distribution system with unbalanced laterals. Without loss of generality, voltage regulators were assumed as fixed in the nominal position. Four different PF algorithms were considered, namely, DS, SAM, BFS, and the formulation proposed in [13] adapted to three-phase networks (3PL). The convergence criterion $\epsilon = 10^{-6}$ has been assumed for all algorithms. In this case, the sensitivity of the formulations' performance to the initializing value and the effect of different ZIP load model combinations will be assessed. As a remark, the 3PL formulation presented similar characteristics to a traditional NR in [13].

5.2.1. Sensitivity to the initializing value $\boldsymbol{V}^0$

For simplicity, let

$$\xi^s = \max_{i\in d,\phi\in\Omega_\Phi} \left\| \mathrm{V}^{0s}_{i,\phi} - V_{i,\phi} \right\| / \left\| \mathrm{V}^{0s}_{i,\phi} \right\|, \quad \forall\, s \in \mathcal{N} \tag{22}$$

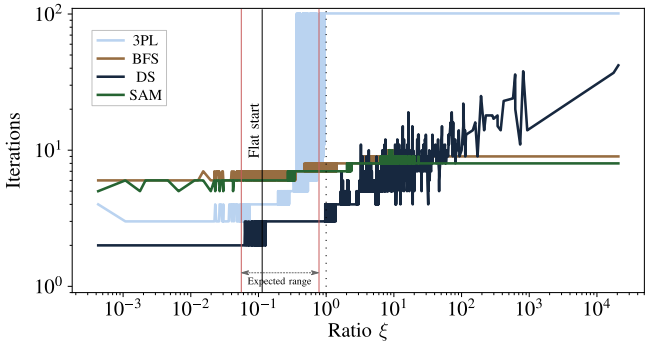

Fig. 4. Power flow performance for different initializing points.

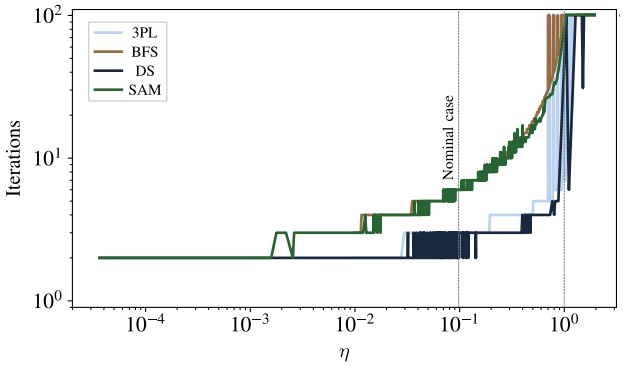

Fig. 5. Power flow performance for different load model combinations.

define the ratio of the boundary as in (6) for each random realization s within a specified number of scenarios $\mathcal{N} = \{1, 2, \ldots, N\}$. Random values were associated to the initializing point as $\mathrm{V}^{0s}_{i,\phi} = \mathcal{V}^s_{i,\phi}\angle\theta^s_{i,\phi}, \forall\, s \in \mathcal{N}$, where $\mathcal{V}^s_{i,\phi} \sim \boldsymbol{U}\left(10^{-12}, 3.0\right)$ and $\theta^s_{i,\phi} \sim \boldsymbol{U}\left(-40°, 40°\right)$ follow uniform distributions. The operational point was arbitrarily assumed for loads and R/X ratio ($\lambda = \rho = 1.0$); hence, $V_{i,\phi}$ is fixed corresponding to $\eta = 0.1142$. The maximum number of iterations was defined as $K = 100$ and the number of scenarios as $N = 10{,}000$. The number of iterations for the algorithms to converge as a function of ξ is displayed in Fig. 4. It can be seen that a flat-start provides a ratio of $\xi = 0.1052$, for which the DS converges in 2 iterations, the 3PL in 3, the SAM in 6, and the BFS in 7. Notice that the 3PL algorithm presents convergence problems around $\xi > 0.4$, while the other algorithms are able to find a solution. However, it must be pointed out that although the DS algorithm converged within the iterations limit for $\xi > 1.0$, it was not always to the same solution. On the other hand, the SAM and BFS did not present convergence problems and converged to the same solution independently on the initial value. This result is an application of Proposition 2 for the SAM algorithm and shows its independence on the initial value. Finally, it is worth mentioning that the DS, SAM, and the BFS did not present any convergence problems within the *expected range* of the initial value ($0.8 < \mathcal{V}^s_{i,\phi} < 1.2$) always converging to the same solution.

5.2.2. Sensitivity to the load model

Random values were associated to the load ZIP components as $\alpha^s_P \sim \boldsymbol{U}\,(0, 1.0)$, $\alpha^s_I = \boldsymbol{U}\,(-1.0, 1/3)$, and $\alpha^s_Z = 1 - \alpha^s_P - \alpha^s_I, \forall\, s \in \mathcal{N}$, following uniform distributions. Such range values are consistent with field measurement reports [28]. Random loading conditions were also assumed within the stable region as $\lambda^s \sim \boldsymbol{U}\,(0.5, 2.8)$. Values were arbitrarily assumed for the R/X ratio ($\rho = 1.0$) and a flat-start was used as initial point. The nominal case consists on $\alpha_P = \lambda = 1.0$. The maximum number of iterations was defined as $K = 100$ and the number of scenarios as $N = 10{,}000$. From (17) it can be seen that the load

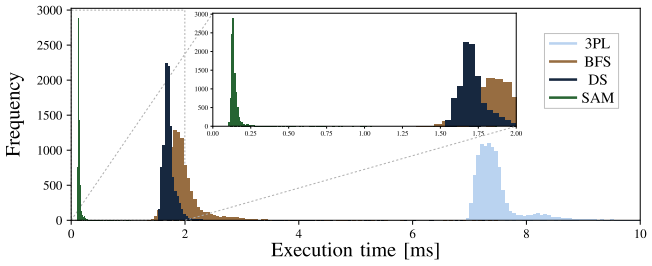

Fig. 6. Execution time per iteration — 123 node test system.

model affects the value of η directly in the numerator and indirectly in the denominator. Hence, the number of iterations for the algorithms to converge as a function of η is displayed in Fig. 5. It can be seen that the nominal case has an $\eta = 0.1142$, presenting the same results described in the previous section. In addition, the dependence on the loading model of the SAM and BFS algorithms is evidenced in Fig. 5, backing up the proof of Proposition 2. However, notice that the BFS and the 3PL presented convergence problems around $\eta > 0.7$, whereas the SAM diverges for $\eta > 1.0$, as deducted from (21). Finally, it must be pointed out that the DS converged under some loading points where $\eta > 1.0$ since in those cases $\alpha_P \approx 0$.

5.3. Computational burden

Tests were performed for the IEEE 123-node test feeder for the nominal case. From the obtained results, the DS and 3PL algorithms display the highest rates of convergence among the tested approaches. However, the time per iteration is considerably higher in the 3PL formulation, as can be seen in Fig. 6, where the histograms of the execution times per iteration are displayed after running 10,000 PF instances for the same operating point with different initializing values. It can be seen that the fastest algorithm is the SAM with an average time per iteration of 0.21 ms, followed by the DS with 1.74 ms, the BFS with 1.97 ms, and finally the 3PL with 7.49 ms. The main driver for these time differences is the number of operations required by each algorithm. Let $\kappa = |d||\Omega_\Phi|$ define the number of equations that need to be solved in the PF. Then, the PF solution with the DS or 3PL algorithms requires solving a system of 2κ equations, whereas the SAM relies on a matrix–vector multiplication of size κ, demanding a lower computational complexity per iteration. Notice also that the fundamental difference of time between the DS and 3PL is the number of internal operations, as can be seen by inspection in [13].

A summary of the computational time required by the tested algorithms is shown in Table 1, where the average total time, average time per iteration, and the average number of iterations is displayed for a single operating point with $\eta \approx 0.05$ and different initial points inside the expected range. Results were obtained for the described tested systems (balanced and unbalanced), including the EPRI feeder K1 in [29], which is a radial, unbalanced 13 kV system with 650 buses and a nominal load of 6 MW, and a representation of the 3120-bus Polish transmission system consisting on 400, 220 and 110 kV network equivalents [30]. In Table 1 it can be seen that the computational burden per iteration in the more comprehensive case ($\kappa = 3120$) is at least three times lower using the SAM algorithm than the DS and 12 times lower than the BFS. Moreover, it can be seen that the 3PL was not able to converge for this test case. Notice that the SAM algorithm is computationally the most efficient in terms of execution times as long as the operation point remains far from the maximum loading condition, i.e., $\eta \ll 1.0$ since the rate of convergence is highly dependent on this parameter, as can be seen in Fig. 5.

Table 1
Average computational results.

κ	Average	DS	SAM	BFS	3PL
33	Total time [ms]	0.4408	0.0739	0.6248	0.7384
	Time/iter. [ms]	0.1880	0.0149	0.1223	0.1510
	Iterations	2.34	4.99	5.07	4.89
99	Total time [ms]	1.2190	0.2169	1.0374	1.6762
	Time/iter. [ms]	0.4269	0.0376	0.1849	0.5587
	Iterations	2.86	5.64	5.63	3.00
135	Total time [ms]	1.4640	0.2267	1.8773	4.1967
	Time/iter. [ms]	0.5123	0.0437	0.3129	0.8368
	Iterations	2.86	5.07	5.80	5.01
357	Total time [ms]	5.0544	1.0249	11.7294	22.4750
	Time/iter. [ms]	1.7447	0.2065	1.9682	7.4917
	Iterations	2.91	4.96	5.37	3.00
1,947	Total time [ms]	58.9358	31.6269	362.5343	1,386.60
	Time/iter. [ms]	17.9239	4.5415	57.1974	419.5348
	Iterations	3.11	6.14	6.32	3.31
3,120	Total time [ms]	169.9171	68.2701	906.4752	–
	Time/iter. [ms]	38.8961	11.3581	147.3772	–
	Iterations	4.40	5.92	6.11	–

6. Conclusions

This paper proposed a novel PF formulation for electrical distribution systems using the CIM and applying the Laurent series expansion. Two solution algorithms were introduced: a Newton-like iterative procedure named direct solution and a successive approximation method. The convergence analysis of the SAM was proven via the Banach fixed-point theorem, ensuring numerical stability and the uniqueness of the solution as long as the system's operating condition is not at the maximum loading point. Results showed that the SAM's rate of convergence depends on the loading point and the branches' impedance, decreasing as $\eta \sim 1.0$. Similarly, it was found that the DS algorithm has a higher rate of convergence as long as $\xi < 1.0$. On the other hand, it was shown that the SAM is independent of the initializing point and is computationally more efficient than the compared algorithms. It was found that the DS is at least three times faster than the BFS algorithm, while the SAM is more than three times faster than the DS. These results validate the scalability and numerical stability of the proposed algorithms. Furthermore, the computational efficiency of the SAM formulation makes it an attractive option for problems in which the PF is solved recursively, such as using metaheuristics, probabilistic analysis, reinforcement learning applied to power systems, among many others [31].

CRediT authorship contribution statement

Juan S. Giraldo: Conceptualization, Methodology, Software, Validation, Writing – original draft. **Oscar Danilo Montoya:** Software, Formal analysis, Writing – review & editing. **Pedro P. Vergara:** Writing – review & editing. **Federico Milano:** Validation, Writing – review & editing.

Declaration of competing interest

The authors declare that they have no known competing financial interests or personal relationships that could have appeared to influence the work reported in this paper.

Acknowledgments

J. S. Giraldo was financially supported by the Netherlands Enterprise Agency (RVO) – DEI+ project 120037 "*Het Indië terrein: Een slimme buurtbatterij in de oude weverij*".

F. Milano was supported by Sustainable Energy Authority of Ireland (SEAI), under the project FRESLIPS, Grant No. RDD/00681.

References

[1] E. Bompard, E. Carpaneto, G. Chicco, R. Napoli, Convergence of the backward/forward sweep method for the load-flow analysis of radial distribution systems, Int. J. Electr. Power Energy Syst. 22 (7) (2000) 521–530.

[2] F. Milano, Continuous Newton's method for power flow analysis, IEEE Trans. Power Syst. 24 (1) (2009) 50–57.

[3] A. Monticelli, A. García, O.R. Saavedra, Fast decoupled load flow: hypothesis, derivations, and testing, IEEE Trans. Power Syst. 5 (4) (1990) 1425–1431.

[4] C. Cheng, D. Shirmohammadi, A three-phase power flow method for real-time distribution system analysis, IEEE Trans. Power Syst. 10 (2) (1995) 671–679.

[5] P.A. García, J.L.R. Pereira, S. Carneiro, V.M. Da Costa, N. Martins, Three-phase power flow calculations using the current injection method, IEEE Trans. Power Syst. 15 (2) (2000) 508–514.

[6] M. Tostado-Véliz, S. Kamel, F. Jurado, Power flow solution of ill-conditioned systems using current injection formulation: Analysis and a novel method, Int. J. Electr. Power Energy Syst. 127 (2021) 106669.

[7] F. Milano, Implicit continuous Newton method for power flow analysis, IEEE Trans. Power Syst. 34 (4) (2019) 3309–3311.

[8] L. Braz, C. Castro, C. Murati, A critical evaluation of step size optimization based load flow methods, IEEE Trans. Power Syst. 15 (1) (2000) 202–207.

[9] P.-J. Lagacé, M.-H. Vuong, I. Kamwa, Improving power flow convergence by Newton raphson with a levenberg-marquardt method, in: 2008 IEEE Power and Energy Society General Meeting-Conversion and Delivery of Electrical Energy in the 21st Century, IEEE, 2008, pp. 1–6.

[10] M. Tostado-Véliz, S. Kamel, F. Jurado, Comparison of various robust and efficient load-flow techniques based on Runge–Kutta formulas, Electr. Power Syst. Res. 174 (2019) 105881.

[11] G.A. Korn, T.M. Korn, Mathematical Handbook for Scientists and Engineers: Definitions, Theorems, and Formulas for Reference and Review, Dover Publications, 2000, pp. 187–220.

[12] A. Garces, A linear three-phase load flow for power distribution systems, IEEE Trans. Power Syst. 31 (1) (2016) 827–828.

[13] O.D. Montoya, L.E. Rueda, W. Gil-González, A. Molina-Cabrera, H.R. Chamorro, M. Soleimani, On the power flow solution in AC distribution networks using the laurent's series expansion, in: 2021 IEEE Texas Power and Energy Conference, TPEC, 2-5 Feb. 2021, College Station, TX, USA, 2021.

[14] S. Bolognani, S. Zampieri, On the existence and linear approximation of the power flow solution in power distribution networks, IEEE Trans. Power Syst. 31 (1) (2016) 163–172.

[15] M. Bazrafshan, N. Gatsis, Convergence of the Z-Bus method for three-phase distribution load-flow with ZIP loads, IEEE Trans. Power Syst. 33 (1) (2018) 153–165.

[16] A. Bernstein, C. Wang, E. Dall'Anese, J.-Y. Le Boudec, C. Zhao, Load flow in multiphase distribution networks: Existence, uniqueness, non-singularity and linear models, IEEE Trans. Power Syst. 33 (6) (2018) 5832–5843.

[17] O.D. Montoya, W. Gil-González, On the numerical analysis based on successive approximations for power flow problems in AC distribution systems, Electr. Power Syst. Res. 187 (2020) 106454.

[18] K.P. Guddanti, Y. Weng, B. Zhang, A matrix-inversion-free fixed-point method for distributed power flow analysis, IEEE Trans. Power Syst. 37 (1) (2022) 653–665.

[19] O.D. Montoya, J.S. Giraldo, L.F. Grisales-Noreña, H.R. Chamorro, L. Alvarado-Barrios, Accurate and efficient derivative-free three-phase power flow method for unbalanced distribution networks, Computation 9 (6) (2021) 61.

[20] W.-M. Lin, Y.-S. Su, J.-H. Teng, S.-J. Chen, A new building algorithm for Z-matrix, in: PowerCon 2000. 2000 International Conference on Power System Technology. Proceedings, Vol. 2, Cat. No. 00EX409, IEEE, 2000, pp. 1041–1046.

[21] J.S. Giraldo, Current injection method using laurent series expansion, 2022, https://github.com/juan-giraldo-ch/CIMLaurent.git. [Online; Accessed February 2022].

[22] A.M. Kettner, M. Paolone, On the properties of the compound nodal admittance matrix of polyphase power systems, IEEE Trans. Power Syst. 34 (1) (2019) 444–453.

[23] J.S. Giraldo, J.A. Castrillón, C.A. Castro, Robust and efficient voltage stability margin computation using synchrophasors, in: 2015 IEEE Power Energy Society General Meeting, 2015, pp. 1–5.

[24] C. Wang, A. Bernstein, J.-Y. Le Boudec, M. Paolone, Explicit conditions on existence and uniqueness of load-flow solutions in distribution networks, IEEE Trans. Smart Grid 9 (2) (2018) 953–962.

[25] LaPSEE Power System Test Cases Repository UNESP, Downloads / sistemas testes, 2020, https://bit.ly/2IdSn91. [Online; (Accessed October 2020)].

[26] J.R. Mantovani, F. Casari, R.A. Romero, Reconfiguração de sistemas de distribuição radiais utilizando o critério de queda de tensão, Controle Automação (2000) 150–159.

[27] F. Milano, A python-based software tool for power system analysis, in: 2013 IEEE Power Energy Society General Meeting, 2013, pp. 1–5.

[28] A. Arif, Z. Wang, J. Wang, B. Mather, H. Bashualdo, D. Zhao, Load modeling—A review, IEEE Trans. Smart Grid 9 (6) (2018) 5986–5999.

[29] Elecrtrical Power System Research Institute, Distributed PV monitoring and feeder analysis - Feeder K1, 2021, URL https://dpv.epri.com/feeder_k.html.

[30] D. POWER, Polish system during morning peak conditions in summer of 2008, 2021, URL https://bit.ly/3D95QH9.

[31] M. Salazar, J.S. Giraldo, P.P. Vergara, P. Nguyen, A. van der Molen, H. Slootweg, Community energy storage operation via reinforcement learning with eligibility traces, in: 2022 Power Systems Computation Conference, PSCC, 2022, in press.